Processing and Application of Ceramics 17 [4] (2023) 400–409
https://doi.org/10.2298/PAC2304400X

Electrical properties and degradation behaviour of BNT-BT-LN ceramics

Qi Xu[1,*], Xuerui Yan[1], Zhiqiang Zhu[1], Hanxing Liu[2]

[1]*College of Materials and Chemistry & Chemical Engineering, Chengdu University of Technology, Chengdu 610059, China*
[2]*State Key Laboratory of Advanced Technology for Materials Synthesis and Processing, School of Material Science and Engineering, Wuhan University of Technology, Wuhan 430070, China*

Received 23 July 2023; Received in revised form 19 November 2023; Accepted 7 December 2023

Abstract

In this paper, phase composition, microstructure, dielectric, ferroelectric and failure behaviour of lead-free (1-x)($Bi_{0.5}Na_{0.5}TiO_3$-$BaTiO_3$)-x$LiNbO_3$ (BNT-BT-LN, x = 0.01, 0.03, 0.05, 0.07 and 0.10) ceramics were investigated. The introduction of $LiNbO_3$ did not change the original perovskite crystal structure of the ceramics with the coexistence of rhombohedral and tetragonal phases. However, with the increase of x (i.e. LN content), the characteristic split XRD peaks became more and more symmetrical. It was observed by scanning electron microscopy that the growth of ceramic grain size was promoted with the increase of LN content. The dielectric temperature stability was also effectively improved with addition of LN. When x = 0.07, the temperature coefficient of capacitance ($TCC_{150\,°C}$) was below ±15% in temperature range of 35–400 °C with moderate permittivity ($\varepsilon_{r150\,°C}$ = 2050) and low dielectric loss ($\tan\delta_{150\,°C}$ = 0.005). The RC time constant of this sample was higher than 19.3 s at temperatures up to 245 °C. The mean time to failure (TTF) empirical formula for the BNT-BT-LN dielectrics was established through highly accelerated life test. As predicted, the TTF could reach 4.67×10^6 h under the applied electric field of 7 kV/mm at room temperature.

Keywords: *BNT-BT, $LiNbO_3$, dielectric temperature stability, ferroelectric properties, mean time to failure*

I. Introduction

In recent years, the miniaturization and lightweight design concept of electronic components and their diversification of application fields put forward more stringent requirements for the high temperature electrical performance and resistance stability of dielectric materials [1]. It has become clear that electronic components that can operate at environment temperatures above 150–200 °C without external cooling support a series of important applications, such as power modules in drilling equipment and engines [2]. A variety of dielectric ceramic systems have been reported for high temperature dielectric capacitors, including $BaTiO_3$ [3,4], $(K_{0.5}Na_{0.5})NbO_3$ [5] and $PbZrO_3$ based systems [6–9]. Among them, lead-free $Bi_{0.5}Na_{0.5}TiO_3$-$BaTiO_3$ (BNT-BT) multi-component solid solution dielectric ceramics are considered as one of the new and promising candidates because of their large dielectric constant and wide operating temperature window [10].

The resistance degradation of dielectrics or capacitors is a process in which the leakage current of dielectric material changes with time under the action of applied electric field [11]. Traditionally, the dielectrics are applied under the voltage and temperature conditions close to the actual application until they fail, and then the mean time to failure (*TTF*) is recorded. This approach is extremely time-consuming, taking weeks to months to complete a set of tests. It takes even longer to evaluate the effects of different experimental conditions on the lifetime of capacitors. HALT (highly accelerated life test) technology overcomes the above shortcomings. High temperature and high voltage are applied on the sample to greatly shorten the failure time. Then, through establishing empirical formula, the *TTF* under any condition can be predicted.

In this work, a series of BNT-BT ceramics modified with $LiNbO_3$ (LN) were fabricated using high tempera-

*Corresponding author: tel: +86 13258275904,
e-mail: *xuqi17@cdut.edu.cn*

Table 1. Composition, sintering temperature and density of BNT-BT-LN ceramic samples

Sample name	Composition		Sintering temperature [°C]	Bulk density [g/cm^3]	Relative density [%TD]
	Proportion of BNT-BT [mol%]	Proportion of LN [mol%]			
LN-1	99	1	1140	5.83	97.3
LN-2	97	3	1080	5.84	97.9
LN-3	95	5	1080	5.78	97.4
LN-4	93	7	1080	5.72	97.3
LN-5	90	10	1080	5.64	96.7

ture solid state reaction method. We focused on the effects of $LiNbO_3$ addition on dielectric properties and temperature stability in the range from room temperature to 400 °C. The degradation of the insulation resistance of BNT-BT-LN dielectrics was also analysed by HALT.

II. Experimental

(1-x)(0.92$Bi_{0.5}Na_{0.5}TiO_3$-0.08$BaTiO_3$)-$x$$LiNbO_3$ (x = 0.01, 0.03, 0.05, 0.07 and 0.10 with sample notation L1, L2, L3, L4 and L5, respectively) ceramics were synthesized by high-temperature solid state reaction method. Firstly, the reagent grade powders TiO_2 (98.5%), Bi_2O_3 (99.0%), $BaCO_3$ (99.0%), Na_2CO_3 (99.8%), Nb_2O_5 (99.5%) and Li_2CO_3 (98.0%) were weighed according to the designed compositions. After ball milling for 24 h in nylon jars, the mixed raw materials were calcined at 800 °C for 2 h, pressed into round blocks and sintered at 1080–1140 °C for 2 h.

X-ray powder diffraction with Cu Kα radiation (PANalytical X'Pert PRO, Holland) and laser Raman spectrometer (Horiba HR Evolution, France) were used to determine the phase purity and crystal structure. Densities of the samples were measured by the principle of Archimedes' method. The scanning electron microscopy (Quanta 450 FEG, USA) and energy dispersive X-ray spectroscopy were used to characterize the morphology of the grains and the elemental distribution. The impedance analyser (Agilent E4980A, USA) was used to measure the dielectric properties. The ferroelectric workstation (HVI0403-239, Radiant Technology, USA) was used to measure the ferroelectric properties. The discharge energy-storage density (W_r) and the charge energy-storage density (W') were evaluated according to the following equation:

$$W = \int_0^E E \, dP \tag{1}$$

where E is applied electric field and P is polarization. The energy-storage efficiency (η) can be calculated by:

$$\eta = \frac{W_r}{W'} \tag{2}$$

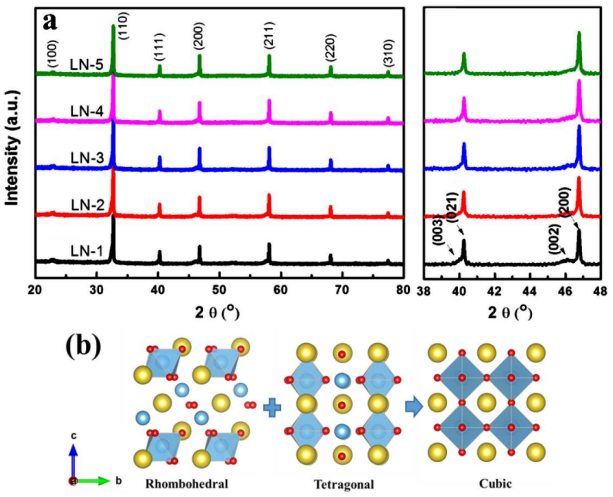

Figure 1. XRD patterns of prepared BNT-BT-LN ceramics (a) and schematic diagram of the corresponding crystal structure (b)

III. Results and discussion

3.1. Structure characterization

All the BNT-BT-LN ceramic samples can be well sintered at 1080–1140 °C with the relative density above 96.7 %TD, as listed in Table 1.

XRD patterns (2θ = 20°–80°) of the BNT-BT-LN ceramics, presented in Fig. 1a, confirm that only a pure perovskite structure can be identified and no secondary impurity was found. It is indicated that in the studied composition range, BT and LN completely diffused into BNT lattice to form solid solutions. From the enlarged diffraction patterns (2θ = 38°–48°), the split peaks (003)/(021) at 2θ = 39°–41° and (002)/(200) at 2θ = 46°–47° could be observed in the sample LN-1. The result corresponded to the coexistence of rhombohedral and tetragonal phases, which was similar to other reported BNT-based ceramic systems [12]. With the increase of x (i.e. LN content), the (003)/(021) and (002)/(200) split peaks became more and more symmetrical. For the composition LN-5, the peaks gradually merged into single peak, exhibiting pseudo cubic structure. The crystal lattice structures were illustrated in Fig. 1b. The "rhombohedral + tetragonal → pseudo cubic" phase structure transition behaviour in BNT-based ceramics with the introduction of a second or third solid solution end-member has been extensively reported [13,14]. It is considered to be caused by the decline of the polar rhombohedral phase and the weakly polar tetragonal phase.

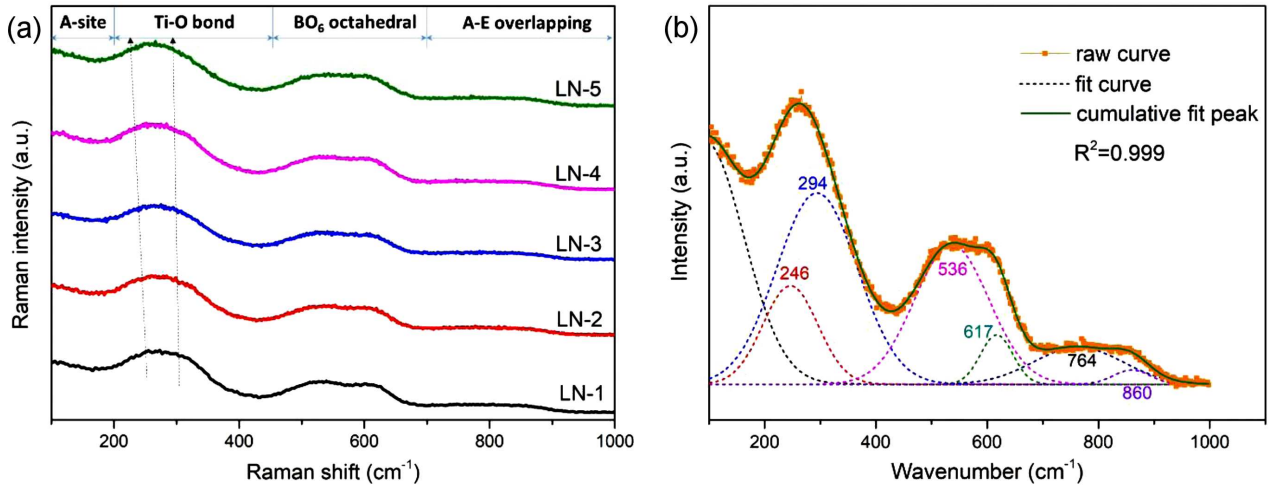

Figure 2. Raman spectra of BNT-BT-LN ceramics (a) and fitting of LN-5 Raman spectra with Gaussian function (b)

To further identify the local structure evolution with varying LN content, the Raman spectroscopy for the BNT-BT-LN ceramics was measured at ambient temperature and fitted using Gaussian function, (Fig. 2). All Raman modes showed broad spectra due to the relaxor ferroelectric nature of BNT-BT-LN ceramics. Four peak regions can be observed in each sample. The first mode was located below 200 cm^{-1}, which was related to the A-site vibration of perovskite [15], including Bi^{3+}, Na^{+}, Ba^{2+} and Li^{+} ions in BNT-BT-LN ceramics. The second mode was approximately in the range of 200–450 cm^{-1}. It is believed that it is associated with the Ti–O bonds vibration [16]. The third peak region from 450 to 700 cm^{-1} was related to the BO_6 octahedra vibration [17] and the fourth mode region >700 cm^{-1} was connected to the A_1 (longitudinal optical) and E (longitudinal optical) overlapping bands [18]. To observe the spectra more intuitively, they were decon-

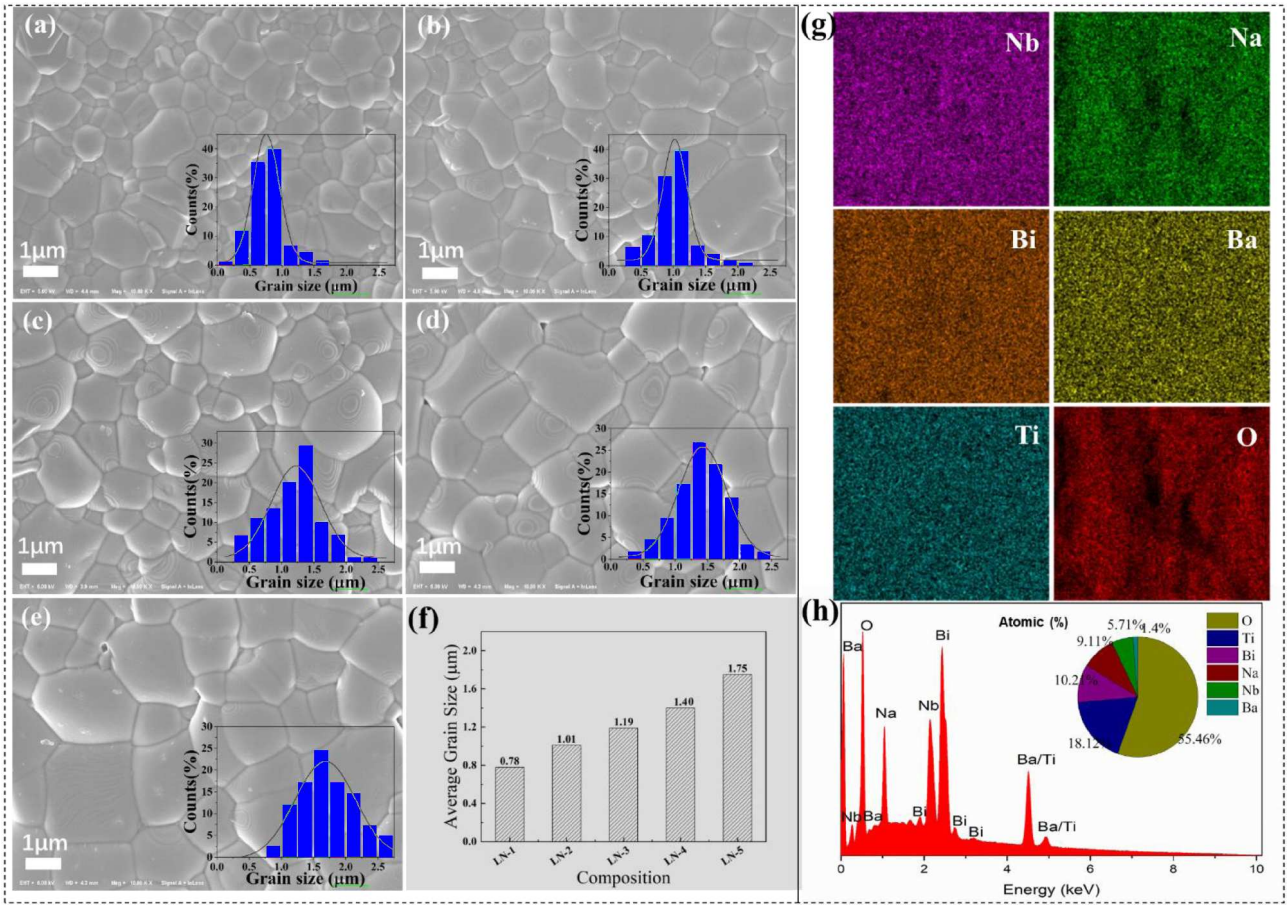

Figure 3. Cross-section SEM images and the corresponding grain size distribution (a-e) and average grain sizes (f) of BNT-BT-LN ceramics; element mapping images and elemental composition (g,h) of 0.93(BNT-BT)-0.07LN (LN-4) ceramics

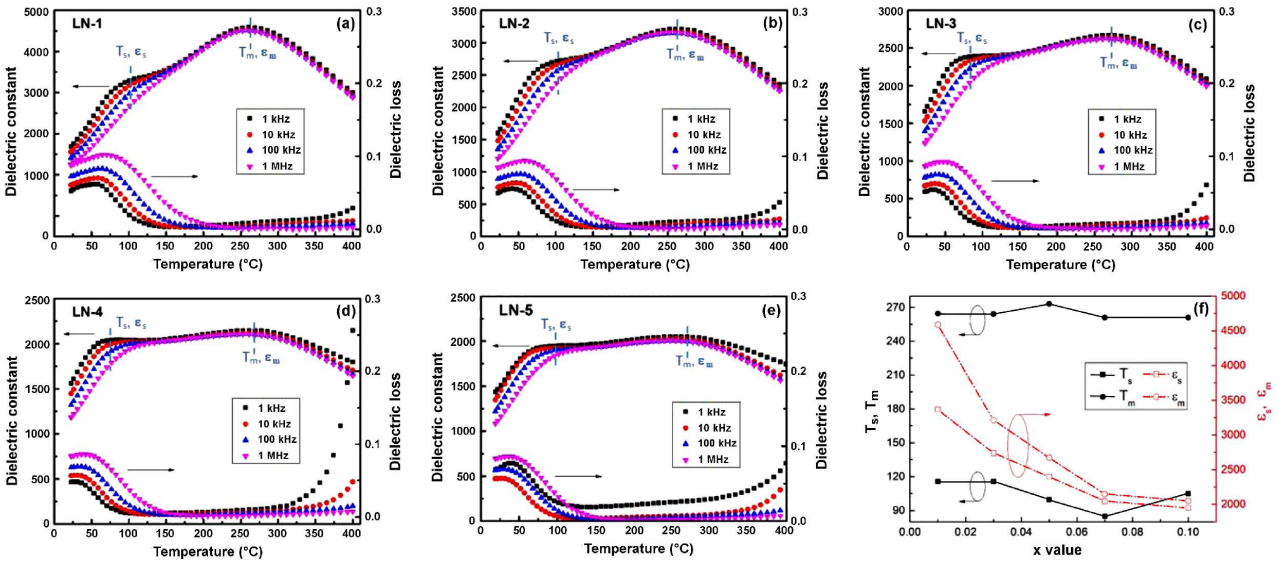

Figure 4. Temperature dependent permittivity of BNT-BT-LN ceramic samples at different frequencies (a-e) and the variation of T_m, T_s, ε_m, ε_s with LN content (f)

voluted into seven peaks based on the Gaussian function. All *R*-square coefficients of the fitted data were higher than 99.9%. With increasing LN content, there was no significant difference in the Raman spectra of the high-frequency overlapping bands in the range 450–1000 cm^{-1}, while the Ti–O bond vibration peak shifted slightly downward. In addition, the peaks revealed a tendency towards broadening with LN addition due to the formation of weak polarity unit cell in the pseudo-cubic matrix. This is thought to be related to the augmentation of structure disorder caused by the introduction of elements (Ba, Li, Nb) at A- and B-sites [19]. As a result, the long-range ferroelectric orders in BNT-BT-LN ceramics were broken and the polar regions with a decreased size were induced by LN incorporation.

All prepared BNT-BT-LN ceramic samples exhibited low porosity and compact microstructure (Fig. 3). The introduction of $LiNbO_3$ promoted the grain growth. Thus, with the increase of $LiNbO_3$ content from 1 to 5 mol%, the average grain size of the BNT-BT-LN ceramics gradually increased from 0.78 to 1.75 μm. Detailed grain size distribution was presented in the insets of Figs. 3a-e and Fig. 3f. It is believed that the grain growth in BNT-BT based ceramics with the addition of the third component is closely related to the formation of oxygen vacancies [20]. It is known that Bi and Na elements volatilize easily during sintering in BNT based ceramic system, leading to the presence of V'_{Na} and V'''_{Bi} being negatively charged. According to the principle of electrical neutrality, oxygen vacancies $V^{\bullet\bullet}_{O}$ with positive charges appear [21], which facilitates the mass transfer during ceramic sintering, thus promoting grain growth. The element mapping and elemental composition of the 0.93(BNT-BT)-0.07LN (LN-4) ceramics were illustrated in Figs. 3g,h. It can be seen that Na, Bi, Ba, Ti, Nb and O elements were uniformly distributed in the selected region without evident component segregation.

3.2. *High-temperature dielectric properties*

Permittivity at room temperature for all the compositions was around 1497–1739 (Fig. 4 a-e) and dielectric loss was lower than 0.072 (Table 2). The frequency dispersion phenomenon and diffuse peak behaviour could be observed, which was regarded as the typical characteristics of relaxor ferroelectrics. Two dielectric peaks at T_s and T_m were clearly observed in the ε_r-T spectra. The subscript *s* stands for "shoulder", while the subscript *m* stands for "maximum". The permittivity at T_s and T_m were indicated as ε_s and ε_m, respectively. The double dielectric anomalies phenomenon was generally recognized in BNT based ceramic systems, which were identified as the thermal evolution and mutual transformation of two kinds of polar nanoregions with different symmetry [22]. It can be seen from Fig. 4f that with the increasing amount of LN, the two characteristic temper-

Table 2. Dielectric properties of BNT-BT-LN ceramics at 1 kHz

Sample	ε_r (at 25 °C)	tan δ (at 150 °C)	ε_r (at 25 °C)	tan δ (at 150 °C)
LN-1	1739	0.054	3562	0.003
LN-2	1647	0.058	2825	0.003
LN-3	1711	0.052	2433	0.002
LN-4	1601	0.048	2050	0.005
LN-5	1497	0.072	1970	0.019

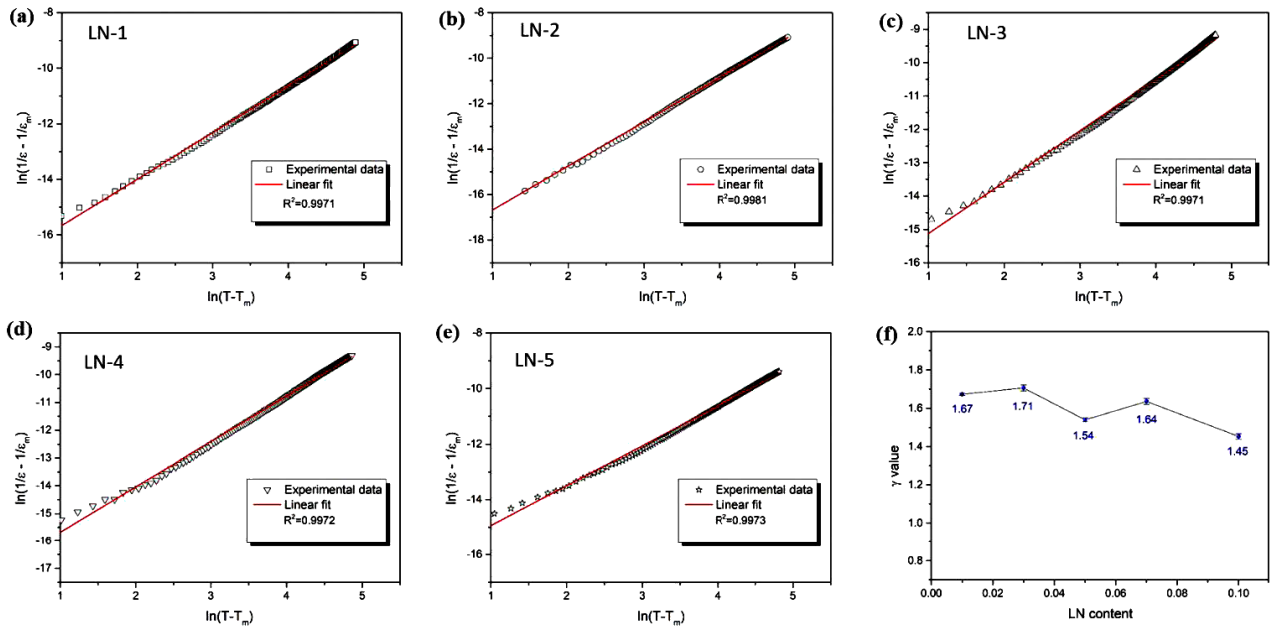

Figure 5. Plots of $\ln(1/\varepsilon - 1/\varepsilon_m)$ versus $\ln(T - T_m)$ at 1 kHz (a-e) and the values of γ with LN (f)

atures T_s and T_m moved towards the direction of low temperature and high temperature, respectively. Meanwhile, both ε_s and ε_m gradually decreased and the dielectric peak became more diffusive, indicating the increase of dielectric relaxation.

The modified Curie-Weiss law has been applied to evaluate the degree of dielectric dispersion:

$$\frac{1}{\varepsilon_r} - \frac{1}{\varepsilon_m} = \frac{(T - T_m)^\gamma}{C} \qquad (\text{at } T > T_m) \qquad (3)$$

where C is the Curie-Weiss constant, ε_r is the permittivity, ε_m is the maximum permittivity and γ is the diffusion parameter. For ideal ferroelectrics and relaxors, the diffusion parameter equals to 1 and 2, respectively. Figures 5a-e show the linear fitting plot of $\ln(1/\varepsilon_r - 1/\varepsilon_m)$ vs. $\ln(T - T_m)$ of the BNT-BT-LN ceramics while the diffusion parameters are given in Fig. 5f. The results revealed that the γ values of all prepared BNT-BT-LN compositions were >1.45, demonstrating that the BNT-BT-LN system had intense relaxor behaviour. At the same time, the flat dielectric platform could guarantee much wider working temperature range.

To investigate the dielectric stability of the BNT-BT-LN ceramics, the temperature coefficient of capacitance (TCC) was calculated by the following equation:

$$TCC = \frac{\Delta C}{C_{150\,^\circ\mathrm{C}}} = \frac{C - C_{150\,^\circ\mathrm{C}}}{C_{150\,^\circ\mathrm{C}}} \qquad (4)$$

where C and $C_{150\,^\circ\mathrm{C}}$ are capacitances at measured temperature and 150 °C, respectively. The capacitance at 150 °C was set as the reference and the corresponding plot was depicted in Fig. 6a. The dashed pink rectangle box indicates the operating temperature range where the variation of TCC value is lower than ±15%. It is worth noting that the compositions with x = 7% (LN-4) and x = 10% (LN-5) exhibited stable permittivity value within a quite wide temperature range from 35 to 400 °C and from 40 to 400 °C. The introduction of $LiNbO_3$ was benefit to the dielectric stability of BNT-BT ceramics, which may be related to the interruption of the long-range ferroelectric order, resulting from the differences in the cation radii and valences at the A- and B-sites of LN and BNT. Additionally, the dielectric loss should be controlled below 0.02 in practical applica-

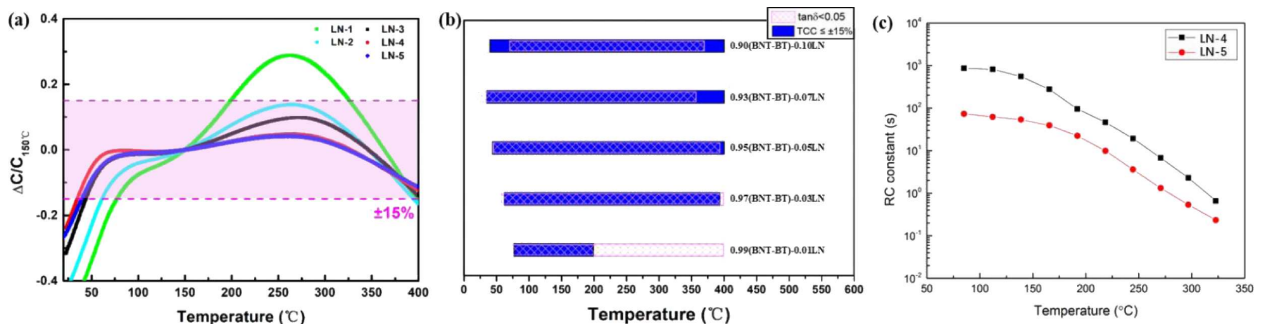

Figure 6. $TCC_{150\,^\circ\mathrm{C}} \leq \pm 15\%$ window (a); temperature stability of ε_r and tan δ (b); RC time constant as a function of temperature for LN-4 and LN-5 samples

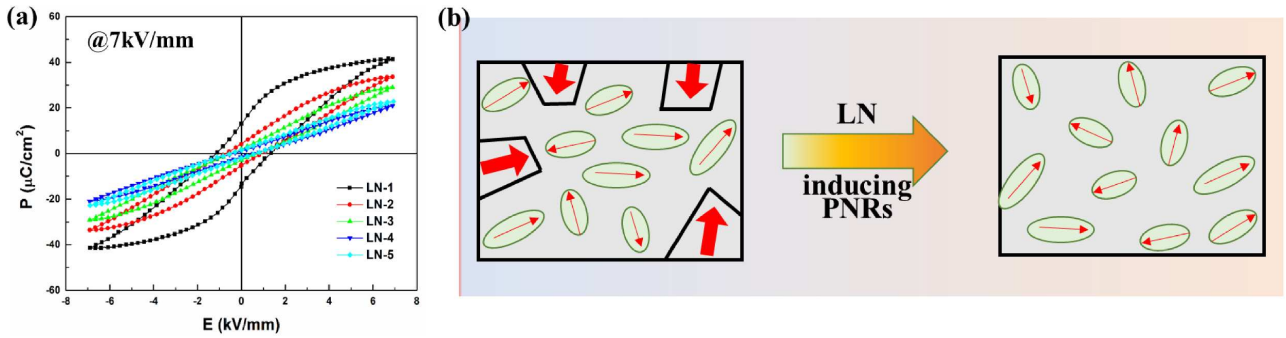

Figure 7. *P-E* loops at 7 kV/mm (a) and schematic representation of ferroelectric order change in BNT-BT-LN ceramics (b)

tions. For the LN-4 and LN-5 samples, the tan δ value at 1 kHz was less than 0.05 in the range 22–357 °C and 71–370 °C, respectively (Fig. 6b), showing great advantages over other materials. Significantly, the dielectric constants for the LN-4 sample at 25 °C and 150 °C are 1601 and 2050, respectively. The dielectric constants for the LN-5 ceramics at 25 °C and 150 °C are 1497 and 1970, respectively. These results show that the BNT-BT-LN ceramics possess great potential for the application in the high temperature systems.

In addition to *TCC*, the *RC* time constant (the product of resistance *R* and capacitance *C*) is also an important parameter in high-temperature capacitors, which measures the ability of dielectrics to maintain charge [23]. From Fig. 6a, it can be obtained that the LN-4 and LN-5 ceramics possess good high temperature stability. Thus, we further characterized their high temperature insulation resistance properties using *RC* constants as shown in Fig. 6c. For the samples LN-4 and LN-5, RC constant was higher than 19.3 s and 3.6 s, respectively, in temperature range up to 245 °C. With the further rise of temperature to 330 °C, the value decreased to 0.23–0.66 s, which was related to the drop in resistivity of the ceramics at higher temperatures.

3.3. Ferroelectric properties

Figure 7a presents the ferroelectric hysteresis loops of the BNT-BT-LN ceramic samples at the electric field of 7 kV/mm. With the increase of LN content, the *P-E* loops became narrower and P_r was close to zero, which revealed the enhancement of the relaxor behaviour. By the introduction of chemical modifier LN, the polar nanoregions dominated in BNT-BT-LN ceramics instead of the long-range ferroelectric orders, as shown in Fig. 7b.

Figure 8a-b shows the *P-E* loops and energy-storage densities of the LN-4 ceramics at 7 kV/mm in frequency range from 1 to 100 Hz. With increasing frequencies, neither P_r nor P_{max} changes significantly, giving rise to stable energy-storage density of 0.58–0.73 J/cm^3 and energy-storage efficiency of 72.4–76.5%. Figure 8c shows the energy-storage characteristics of the BNT-BT-LN ceramics under the critical electric field (E_c). The polarization reduction revealed that more ferroelectric long-range orders were interrupted by LN addition, which confirmed the enhancement of the relaxor behaviour. With the addition of $LiNbO_3$ from 1 to 7 mol%, E_c gradually increased from 10.1 to 12.7 kV/mm. Thus, the maximum effective energy-storage density was largely improved. For the samples LN-2–LN-4, W_r was larger than 1.2 J/cm^3, indicating that the BNT-BT-LN system can obtain a better energy-storage density under medium intensity electric field. Meanwhile, with the increase of LN content, the energy-storage efficiency gradually increased due to the reduction of P_r. Synthetically considering W_r and η, the 0.93(BNT-BT)-0.07LN composition exhibited a maximum energy-storage density of 1.5 J/cm^3 with an efficiency of 70% at 12.7 kV/mm, indicating great potential for ceramic dielectric capacitor applications.

3.4. Degradation of resistance behaviour analysis

Highly accelerated life testing (HALT) system consists of four parts, as shown in Fig. 9a, including the power supply providing high voltage, the oven containing sample stage, the HALT electronics for measuring

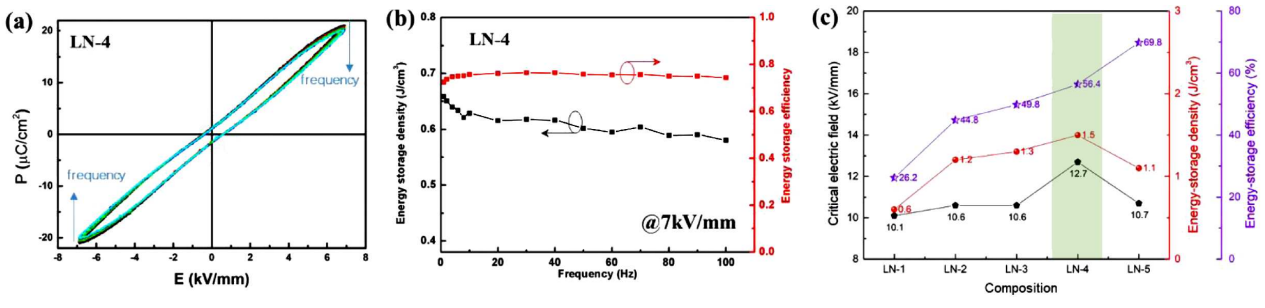

Figure 8. Frequency stability (a) and energy-storage densities and efficiencies (b) of the composition LN-4; energy-storage densities and efficiencies at critical electric field of BNT-BT-LN ceramics (c)

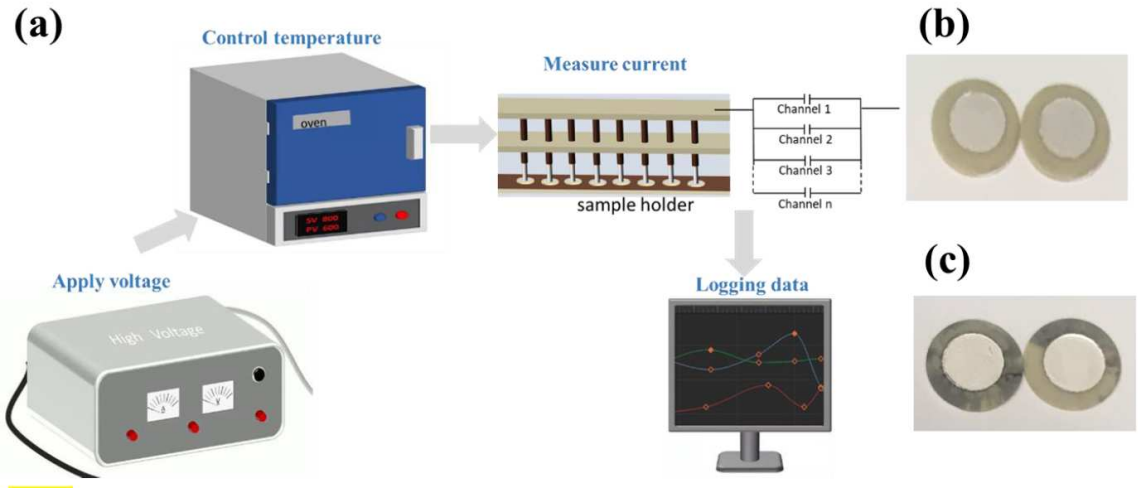

Figure 9. Schematic illustration of HALT testing system (a), pristine samples (b) and failed samples (c)

current and the computer for logging data. The original data collected is the leakage current over time, which is used to determine whether the device or material fails. Up to now, there is no uniform standard for determining the failure time. Currently, it is generally accepted that the failure of devices is judged when the insulation resistance of the device decreases by 30% compared with the initial value. In this work we adopt the criteria that the time when the leakage current increases to one thousand times of the initial value is determined to be the time to failure (*TTF*) [24]. The photos of pristine and failed samples are presented in Figs. 9b,c. Black lines from the electrode edge to the sample edge can be observed on the surface of the ceramic disk after failure.

The empirical formula proposed by Prokopowicz and Vaskas [25] is widely used to characterize HALT analysis:

$$\frac{t_1}{t_2} = \left(\frac{V_2}{V_1}\right)^n \exp\left[\frac{E_A}{k_B}\left(\frac{1}{T_1} - \frac{1}{T_2}\right)\right] \tag{5}$$

where t represents the determined *TTF*, V is the test voltage, n represents voltage acceleration factor, E_A represents the failure activation energy, also known as temperature acceleration factor, k_B is Boltzmann constant and T is the testing temperature, the subscripts 1 and 2 indicate two different testing conditions. Among the above parameters, n and E_A are intrinsic factors being determined by the characteristics of the dielectric or capacitor.

According to the available experimental results, the LN-4 sample possesses the best energy storage performance and high temperature dielectric stability. Thus, the composition LN-4 was selected for the HALT analysis. Figures 10a,b show *TTF* tested at different temperatures from 220 to 280 °C and different voltages from 500 to 900 V. From the data, *TTF* value of the sample declined with the increase of both temperature and voltage. *TTF* of the LN-4 ceramics was linear *vs*. the reciprocal of temperature at the same voltage of 500 V and different temperatures (Fig. 10c). According to the equation:

$$\ln t_2 - \ln t_1 = \frac{E_A}{k_B}\left(\frac{1}{T_1} - \frac{1}{T_2}\right) \tag{6}$$

the failure activation energy E_A was calculated to be 1.14 eV. *TTF* of the LN-4 ceramics was linear *vs*. the logarithm of the voltage at the same temperature of 250 °C and different voltages (Fig. 10d). According to the equation:

$$\ln t_2 - \ln t_1 = -n(\ln V_2 - \ln V_1) \tag{7}$$

the voltage acceleration factor n was calculated to be 2.64.

Generally, capacitors have two failure modes, one is avalanche breakdown (ABD) and the other is thermal runaway (TRA) [26]. The ABD failure mode is when the leakage current increases sharply at a certain moment leading to a sudden breakdown, while the leakage current in the TRA failure mode increases slowly with the increase of time and gradually fails. Obviously, the failure mode of BNT-BT-LN dielectrics should be TRA mode, while the ions or defects involved in TRA can be judged by the failure activation energy. Shih *et al.* [24] reported that in $BaNd_2Ti_4O_{12}$ + ZnO-B_2O_3 ceramic capacitors, the diffusion of Ag ions led to the final failure of capacitors and its failure activation energy reached 1.8 eV. In $BaTiO_3$-based [27–29] and $Ca(Zr,Ti)O_3$-based [2] ceramics, the failure activation energy is generally in the range of 1.1–1.5 eV and the failure mechanism is related to the migration of oxygen vacancy under the action of DC electric field. In this study, the activation energy of the LN-4 sample was calculated to be 1.14 eV as we analysed above. It was believed that the failure process was caused by the electromigration of oxygen vacancies.

Oxygen vacancy is one of the most common defects in dielectric ceramics sintered at high temperature. In HALT test, the positively charged oxygen vacancies $V_O^{\bullet\bullet}$ migrate towards the negative electrode under the action of DC electric field. Although the grain boundary has

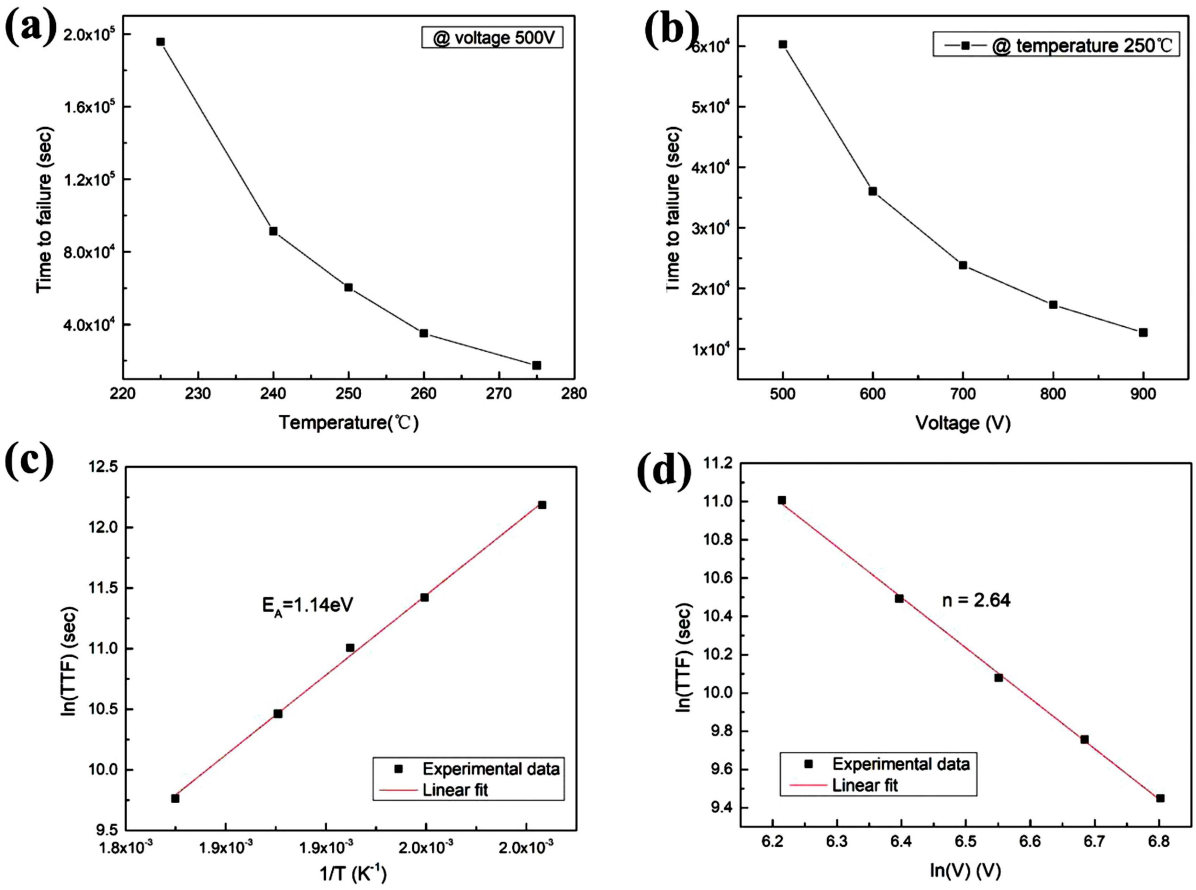

Figure 10. ***TTF*** **at different temperatures and voltages (a,b); calculation of degradation activation energy** E_A **and acceleration factor** n **(c,d) for LN-4 ceramic samples**

a certain barrier effect, some oxygen vacancies can still move across the grain boundary. With the increase of testing time, a greater concentration of oxygen vacancies accumulates near the negative electrode. It leads to a sharp increase in the leakage current and the final failure of the capacitor [29], as shown in Fig. 11.

According to the calculated E_A and n values for the BNT-BT-LN ceramics, *TTF* under any other conditions can be predicted with the following empirical formula:

$$\frac{t_1}{t_2} = \left(\frac{V_2}{V_1}\right)^{2.64} \exp\left[\frac{1.92 \cdot 10^{-19}}{k_B}\left(\frac{1}{T_1} - \frac{1}{T_2}\right)\right] \quad (8)$$

Figure 12 represents the predicted *TTF* values of the 0.93(BNT-BT)-0.07LN ceramics under some common electric fields and temperatures. At 7 kV/mm and room temperature, *TTF* can reach 4.67×10^6 h. With increasing electric field and temperature, the time to failure

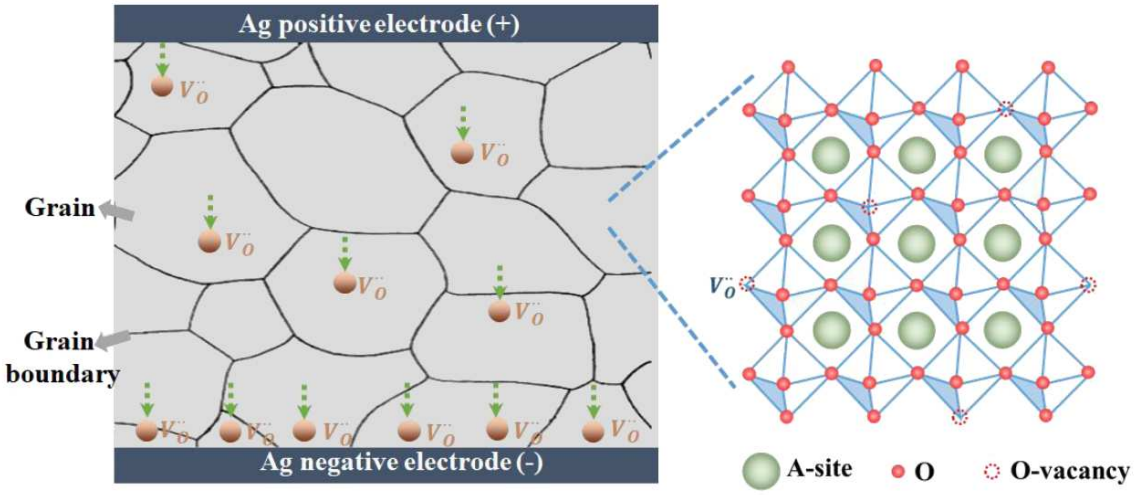

Figure 11. Schematic diagram of oxygen vacancy migration in the degraded BNT-BT-LN ceramics

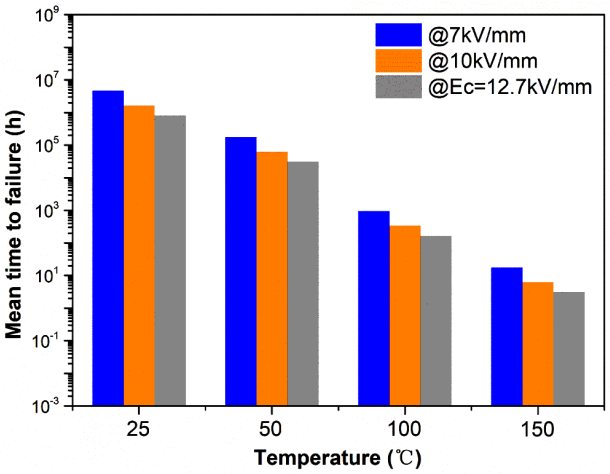

Figure 12. The prediction of mean time to failure for 0.93(BNT-BT)-0.07LN ceramics

keeps decreasing. It is predicted that under the critical electric field of 12.7 kV/mm and at 150 °C, *TTF* drops to 3.05 h. Lee *et al.* [2] studied the degradation behaviour of $Ca(Zr_{0.80}Ti_{0.20})O_3$ monolayer ceramic capacitors with dielectric layer thickness of 50 μm. They predicted that *TTF* was close to 12300 h under the conditions of 1.5 MV/cm and 150 °C. Obviously, the time to failure of the BNT-BT-LN in this study is still lower than that in literature reports, which is mainly caused by the thickness of dielectrics. The degradation behaviour of micron scale dielectrics will be further investigated in our future work.

IV. Conclusions

Dense $(1\text{-}x)(Bi_{0.5}Na_{0.5}TiO_3\text{-}BaTiO_3)\text{-}xLiNbO_3$ (BNT-BT-LN, x = 0.01, 0.03, 0.05, 0.07 and 0.10) ceramics with pure perovskite phase were fabricated by solid-state reaction method. The coexistence of rhombohedral and tetragonal phases was observed, but with the increase of LN content, the characteristic splitting XRD peaks became more and more symmetrical. The average grain size of the BNT-BT-LN ceramic samples gradually increased from 0.78 to 1.75 μm with LN content. For the composition LN-4, the time to failure $TCC_{150\,°C} \leq \pm 15\%$ in the temperature range from 35 to 400 °C. Ferroelectric long-range orders were interrupted by LN, which confirmed the enhancement of the relaxor behaviour. Highly accelerated life testing (HALT) analysis indicated that the failure process of the BNT-BT-LN dielectrics was caused by the electromigration of oxygen vacancies.

Acknowledgement: This work was supported by the National Natural Science Foundation of China (No. 51372191), "Four New Project" curriculum teaching reform project of Chengdu University of Technology (No. 11100-000114-22155). The authors wish to thank Michael T. Lanagan for his support with the HALT measurements.

References

1. C.A. Randall, R. Maier, W. Qu, K. Kobayashi, K. Morita, Y. Mizuno, N. Inoue, T. Oguni, "Improved reliability predictions in high permittivity dielectric oxide capacitors under high dc electric fields with oxygen vacancy induced electromigration", *J. Appl. Phys*., **113** [1] (2013) 014101.
2. H. Lee, J.R. Kim, M.J. Lanagan, S. Trolier-McKinstry, C.A. Randall, "High-energy density dielectrics and capacitors for elevated temperatures: $Ca(Zr,Ti)O_3$", *J. Am. Ceram. Soc*., **96** [4] (2013) 1209–1213.
3. H. Ogihara, C.A. Randall, S. Trolier-Mckinstry, "High-energy density capacitors utilizing $0.7BaTiO_3\text{-}0.3BiScO_3$ ceramics", *J. Am. Ceram. Soc*., **92** [8] (2009) 1719–1724.
4. H. Ogihara, C.A. Randall, S. Trolier-Mckinstry, "Weakly coupled relaxor behavior of $BaTiO_3\text{-}BiScO_3$ ceramics", *J. Am. Ceram. Soc*., **92** [1] (2009) 110–118.
5. H. Du, W. Zhou, F. Luo, D. Zhu, S. Qu, Z. Pei, "Phase structure, dielectric properties, and relaxor behavior of $(K_{0.5}Na_{0.5})NbO_3\text{-}(Ba_{0.5}Sr_{0.5})TiO_3$ lead-free solid solution for high temperature applications", *J. Appl. Phys*., **105** [12] (2009) 124104.
6. X. Hao, J. Zhai, L.B. Kong, Z. Xu, "A comprehensive review on the progress of lead zirconate-based antiferroelectric materials", *Progr. Mater. Sci*., **63** (2014) 1–57.
7. L. Zhang, S. Jiang, B. Fan, G. Zhang, "High energy storage performance in $(Pb_{0.858}Ba_{0.1}La_{0.02}Y_{0.008})(Zr_{0.65}Sn_{0.3}Ti_{0.05})O_3\text{-}(Pb_{0.97}La_{0.02})(Zr_{0.9}Sn_{0.05}Ti_{0.05})O_3$ anti-ferroelectric composite ceramics", *Ceram. Int*., **41** [1] (2015) 1139–1144.
8. G. Zhang, D. Zhu, X. Zhang, L. Zhang, J. Yi, B. Xie, Y. Zeng, Q. Li, Q. Wang, S. Jiang, "High-energy storage performance of $(Pb_{0.87}Ba_{0.1}La_{0.02})(Zr_{0.68}Sn_{0.24}Ti_{0.08})O_3$ antiferroelectric ceramics fabricated by the hot-press sintering method", *J. Am. Ceram. Soc*., **98** [4] (2015) 1175–1181.
9. S. Jiang, L. Zhang, G. Zhang, S. Liu, J. Yi, X. Xiong, Y. Yu, J. He, Y. Zeng, "Effect of Zr:Sn ratio in the lead lanthanum zirconate stannate titanate anti-ferroelectric ceramics on energy storage properties", *Ceram. Int*., **39** [5] (2013) 5571–5575.
10. Q. Xu, H. Liu, J. Xie, L. Zhang, W. Luo, X. Huang, M. Cao, H. Hao, Z. Yao, M.T. Lanagan, "High-temperature dielectrics in BNT-BT based solid solution", *IEEE Trans. Ultrason. Ferroelectr. Freq. Control*, **63** [10] (2016) 1656–1662.
11. X. Zhang, J. Zhang, Y. Zhou, Z. Xie, Z. Yue, L. Li, "Highly accelerated resistance degradation and thermally stimulated relaxation in $BaTiO_3$-based multilayer ceramic capacitors with Y5V specification", *J. Alloys Compd*., **662** (2016) 308–314.
12. Y. Jia, H. Fan, H. Wang, A.K. Yadav, B. Yan, M. Li, Q. Quan, G. Dong, W. Wang, Q. Li, "Large electrostrain and high energy-storage of $(1\text{-}x)[0.94(Bi_{0.5}Na_{0.5})TiO_3\text{-}0.06BaTiO_3]\text{-}xBa(Sn_{0.70}Nb_{0.24})O_3$ lead-free ceramics", *Ceram. Int*., **47** [13] (2021) 18487–18496.
13. G. Viola, H. Ning, X. Wei, M. Deluca, A. Adomkevicius, J. Khaliq, M.J. Reece, H. Yan, "Dielectric relaxation, lattice dynamics and polarization mechanisms in $Bi_{0.5}Na_{0.5}TiO_3$-based lead-free ceramics", *J. Appl. Phys.*, **114** [1] (2013) 014107.
14. G. Viola, R. Mkinnon, V. Koval, A. Adomkevicius, S. Dunn, H. Yan, "Lithium-induced phase transitions in lead-free $Bi_{0.5}Na_{0.5}TiO_3$ based ceramics", *J. Phys. Chem. C*, **118** [16] (2014) 8564–8570.

15. E. Birks, M. Dunce, R. Ignatans, A. Kuzmin, A. Plaude, M. Antonova, K. Kundzins, A. Sternberg, "Structure and dielectric properties of $Na_{0.5}Bi_{0.5}TiO_3$-$CaTiO_3$ solid solutions", *J. Appl. Phys*., **119** [7] (2016) 074102.
16. S.N. Tripathy, K.K. Mishra, S. Sen, D. Pradhan, "Dielectric and Raman spectroscopic studies of $Na_{0.5}Bi_{0.5}TiO_3$-$BaSnO_3$ ferroelectric system", *J. Am. Ceram. Soc*., **97** [6] (2014) 1846–1854.
17. J. Shi, R. Rao, W. Tian, X. Xu, X. Liu, "Anomalous electrical performance of A-site double-bivalent-doped $Bi_{0.49}Na_{0.5}TiO_{3-\delta}$ ceramics from nominal oxygen deficiency to excess", *Ceram. Int*., **48** (2022) 5210–5216.
18. C. Zhu, Z. Cai, B. Luo, L. Guo, L. Li, X. Wang, "High temperature lead-free BNT-based ceramics with stable energy storage and dielectric properties", *J. Mater. Chem. A*, **8** [2] (2020) 683–692.
19. C. Li, J. Liu, W. Bai, S. Wu, P. Zheng, J. Zhang, Z. Pan, J. Zhai, "Superior energy storage performance in $(Bi_{0.5}Na_{0.5})TiO_3$-based lead-free relaxor ferroelectrics for dielectric capacitor application via multiscale optimization design", *J. Mater. Chem. A*, **10** [17] (2022) 9535–9546.
20. Q. Xu, H. Liu, Z. Song, X. Huang, A. Ullah, L. Zhang, J. Xie, H. Hao, M. Cao, Z. Yao, "A new energy-storage ceramic system based on $Bi_{0.5}Na_{0.5}TiO_3$ ternary solid solution", *J. Mater. Sci. Mater. Electron*., **27** [1] (2016) 322–329.
21. M. Zhu, H. Hu, N. Lei, Y. Hou, H. Yan, "Dependence of depolarization temperature on cation vacancies and lattice distortion for lead-free $74(Bi_{1/2}Na_{1/2})TiO_3$–$20.8(Bi_{1/2}K_{1/2})TiO_3$–$5.2BaTiO_3$ ferroelectric ceramics", *Appl. Phys. Lett*., **94** [18] (2009) 182901.
22. W. Jo, S. Schaab, E. Sapper, Lj.A. Schmitt, H.J. Kleebe, A.J. Bell, J. Rödel, "On the phase identity and its thermal evolution of lead free $(Bi_{1/2}Na_{1/2})TiO_3$-6 mol% $BaTiO_3$", *J. Appl. Phys*., **110** [7] (2011) 074106.
23. R. Dittmer, W. Jo, D. Damjanovic, R. Rödel, "Lead-free high-temperature dielectrics with wide operational range", *J. Appl. Phys*., **109** [3] (2011) 034107.
24. Y-T. Shih, J-H. Jean, S-C. Lin, "Failure mechanism of a low-temperature-cofired ceramic capacitor with an inner Ag electrode", *J. Am. Ceram. Soc*., **93** [10] (2010) 3278–3283.
25. T. Prokopowicz, A. Vaskas, "Research and development intrinsic reliability subminiature ceramic capacitors", Final Report, ECOM-90705-F, NTIS AD-864068, 1969.
26. B. Rawal, N. Chan, "Conduction and failure mechanisms in barium titanate based ceramics under highly accelerated conditions", pp. 184–188 in *Proceedings of The 34th Electronic Components Conference*, New Orleans, 1984.
27. S. Sato, Y. Nakano, A. Sato, T. Nomura, "Effect of Y-doping on resistance degradation of multilayer ceramic capacitors with Ni electrodes under the highly accelerated life test", *Jpn. J. Appl. Phys*., **36** (1997) 6016–6020.
28. H. Shizuno, S. Kusumi, H. Saito, H. Kishi, "Properties of Y5V multilayer ceramic capacitors with electrodes", *Jpn. J. Appl. Phys.*, **32** (1993) 4380–4383.
29. G. Yang, G. Lian, E. Dickey, C.A. Randall, D.E. Barber, P. Pinceloup, M.A. Henderson, R.A. Hill, J.J. Beeson, D.J. Skamser, "Oxygen nonstoichiometry and dielectric evolution of $BaTiO_3$. Part II - insulation resistance degradation under applied dc bias", *J. Appl. Phys*., **96** [12] (2004) 7500–7508.